Finite Element Modeling of Ballistic Impact on Kevlar 49 Fabrics

Deju Zhu[1], Barzin Mobasher[2], S.D. Rajan[3]

[1] Postdoctoral fellow, Department of Mechanical Engineering, McGill University, Montreal, QC, Canada, E-mail: Deju.Zhu@mail.mcgill.ca
[2] Professor, Ph.D., P.E., Department of Civil, Environmental and Sustainable Engineering, Arizona State University, Tempe, AZ, 85287, E-mail: Barzin@asu.edu
[3] Professor, Ph.D., Department of Civil, Environmental and Sustainable Engineering, Arizona State University, Tempe, AZ, 85287, corresponding author, E-mail: S.Rajan@asu.edu

ABSTRACT

This paper presents an improved material model suitable for Kevlar 49 fabric which was implemented into the commercial explicit Finite Element (FE) software LS-DYNA through a user defined material subroutine (UMAT). The fabric constitutive behavior in the current material model was obtained from new experimental data in the principal material directions (warp and fill) under static loading. Two different modeling configurations, i.e. single FE layer and multiple FE layers were used to simulate the ballistic tests conducted at NASA Glenn research center. Both the shear properties of the fabric and the parameters used in Cowper-Symonds (CS) model which accounts for strain rate effect on material properties were optimized to achieve close match between the FE simulations and experimental data. The residual velocity of the projectile, the absorbed energy by the fabric after impact, and the temporal evolution and the spatial distribution of the fabric deformation and damage were closely examined. Sensitivity analysis was carried out to study the effect of the failure strain of the fabric and the coefficient of friction on the simulation results.

Keywords: Ballistic impact; Kevlar fabric; Strain rate effect; Finite element model

1. Introduction

Fabrics based on high-performance fibers are extensively employed in variety of ballistic and impact protection applications. Despite the fact that over the past two decades, there has been a great deal of work done on understanding the ballistic behavior of these fabrics using various analytical and numerical techniques, the design of fabric armor systems remains largely based on the employment of extensive experimental test programs and empiricism. While such experimental programs are critical for ensuring the utility and effectiveness of the armor systems, they are generally expensive, time-consuming and involve destructive testing. Consequently, there is a continuing effort to reduce the extent of these experimental test programs by complementing them with the corresponding computation-based engineering analyses and simulations [1].

In our previous study [2], a material model was developed to include non-linearity in the stress-strain response and strain rate effect on the material response. The model was incorporated into the LS-DYNA through a UMAT and was validated by comparing the results against experimental ballistic tests conducted at NASA Glenn Research Center. The fabric layers were represented by one single finite element (FE) layer; hence it was not able to capture the effect of friction between the fabrics layers which is actually an important factor for determining the ballistic behavior of the fabric. Later on, a multi-layer model was built to consider the friction between the fabric layers [3]. But all these models were built on the experimental data where the fabric was loaded up to the strain of about 4% [4, 5], and the post-peak behaviors were assumed to follow certain patterns without experimental validation. New experimental data show that the fabric can deform up to 20% before the complete failure, the energy absorption ability will dramatically increase due to the large strain capacity [6]. Research on the mechanics properties of aramid yarns and woven fabrics has been reported by some authors. Amaniampong and Burgoyne [7] studied the effect of gage length and strain rate from $3x10^{-4}$ to 0.003 s^{-1} on the failure stress and

failure strain of Kevlar® 49 yarns. Yarn strength decreases slightly as the gage length increases; whereas the failure strain of the Kevlar® 49 yarns was independent of the gage length, however decreased slightly as the strain rate increased. Zhu et al. [8-11] conducted dynamic tensile testing on Kevlar® 49 single yarn and fabrics using a servo-hydraulic high speed machine [12-18] and found that the Young's modulus, tensile strength, maximum strain and toughness increased with increasing strain rate over a range of 20 to 170 s^{-1}.

In the current study, the fabric constitutive behavior was obtained from the new experimental data in the principal material directions. Based on the new constitutive behavior, the UMAT was modified and new material parameters were identified for the simulations. Single layer and multi-layer models were used to simulate the ballistic tests conducted at NASA Glenn research center. Finally, sensitivity analysis was carried out to study the effect of failure strain and friction coefficient on the simulation results of the multi-layer model.

2. Constitutive Modeling

2.1 Constitutive Behavior of the Fabric

In this study simplified assumptions were made to fully capture the complexities of the stress-strain behavior in the principal material directions (warp and fill). The fabric has negligible stiffness perpendicular to both fabric material directions and hence those properties were assumed to be zero. No coupling effect between the material directions was assumed – the Poisson's ratios were assumed to be zero. The constitutive behavior used in the material model in stiffness incremental form is shown in Eq. (1):

$$\begin{bmatrix} \Delta\sigma_{11} \\ \Delta\sigma_{22} \\ \Delta\sigma_{33} \\ \Delta\sigma_{12} \\ \Delta\sigma_{31} \\ \Delta\sigma_{23} \end{bmatrix} = \begin{bmatrix} E_{11} & 0 & 0 & 0 & 0 & 0 \\ 0 & E_{22} & 0 & 0 & 0 & 0 \\ 0 & 0 & 0 & 0 & 0 & 0 \\ 0 & 0 & 0 & 2G_{12} & 0 & 0 \\ 0 & 0 & 0 & 0 & 2G_{31} & 0 \\ 0 & 0 & 0 & 0 & 0 & 2G_{23} \end{bmatrix} \begin{bmatrix} \Delta\varepsilon_{11} \\ \Delta\varepsilon_{22} \\ \Delta\varepsilon_{33} \\ \Delta\varepsilon_{12} \\ \Delta\varepsilon_{31} \\ \Delta\varepsilon_{23} \end{bmatrix} \quad (1)$$

Material direction 11 refers to the main longitudinal direction of the fabric or warp direction, direction 22 refers to the direction along the width of the fabric or fill direction, and direction 33 refers to the direction perpendicular to both warp and fill directions. E_{33} is taken as zero simply because shell elements are used to model the fabric. The values for E_{11}, E_{22}, G_{12}, G_{31}, and G_{23} are a function of several factors including current stress and strain, stress and strain history, and strain rate. The determination of these material properties will be discussed in the following section.

2.2 Material Parameters of the Fabric

New tensile tests were conducted in both warp and fill directions until the load carrying capacity of the fabric reached most zero, the results show that the fabric can deform up to 20% before the complete failure. Figures 1(a) and 1(b) show the new stress-strain curves used in the model based on quasi-static tensile test results using 200 mm x 50 mm (length x width) swath specimens and the material model developed for the fabric in warp and fill directions, respectively. Note that there are four distinct regions in the constitutive behavior: crimp region, linear pre-peak region, linear post-peak region and non-linear post-peak region. In the crimp region, the stress increase is relative low due to the straightening of the woven structure of the fabric. When the crimp is removed the straightened yarns start to behavior linearly and take more loads, reaching linear pre-peak region. When the stress level reaches the tensile strength of the fabric the yarns start to break and the stress of the fabric decreases dramatically until reaching a transition point which is about 70 MPa (linear post-peak region). After the transition point the stress decreases gradually to almost zero when the strain reaches to about 0.2 mm/mm, representing the non-linear post-peak region.

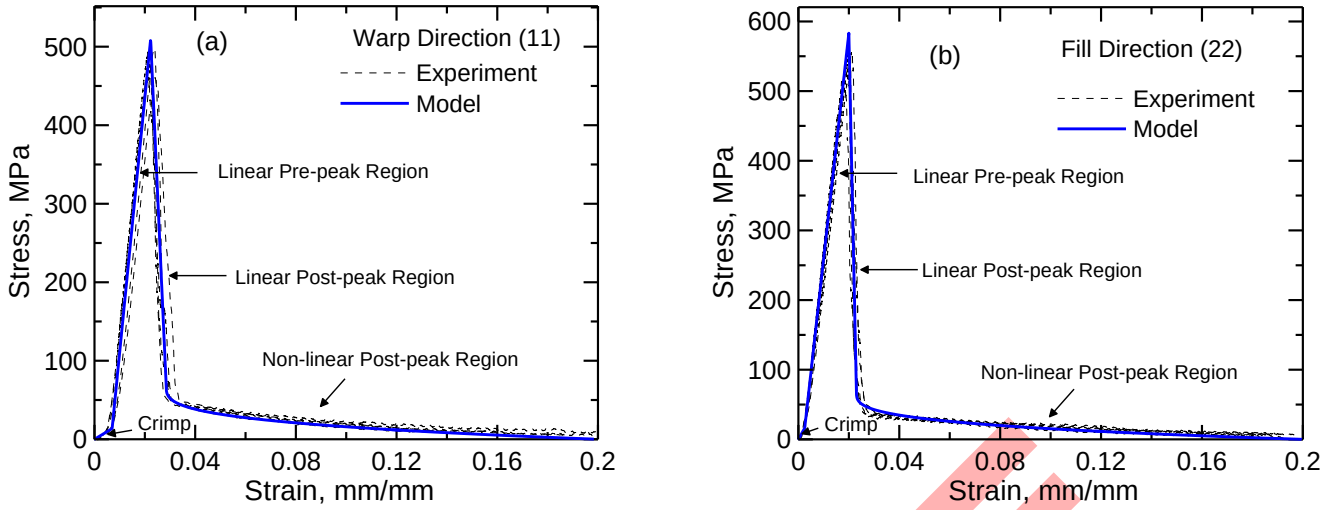

Fig. 1 Stress-strain curves and model in (a) warp and (b) fill directions

Based on the stress-strain curves in the warp and the fill directions, it was found that the elastic stiffness in pre-peak region of warp direction is identical to that of fill direction, and the crimp stiffness for warp and fill directions is 0.06 and 0.20 times of the elastic stiffness in pre-peak region, respectively. The stiffness in linear post-peak region of warp and fill directions is 2.2 and 5.6 times of the elastic stiffness in pre-peak region. The crimp strain of the warp direction is about 2.6 times larger than that of the fill direction. And the peak stress of the warp direction is 15% lower than that of the fill direction. There is a slight difference in the strain at peak stress and the stiffness of linear post-peak region. In the current material model, the elastic stiffness and strain at peak stress were assumed to be a function of the strain rate using Cowper-Symonds model as follows:

$$E_{ii}^{adj} = E_{ii}\left(1+\frac{\dot{\varepsilon}_{ii}}{C_E}\right)^{1/P_E} \tag{2}$$

$$\varepsilon_{ii}^{\max(adj)} = \varepsilon_{ii}^{\max}\left(1+\frac{\dot{\varepsilon}_{ii}^{\max}}{C_\varepsilon}\right)^{1/P_\varepsilon} \tag{3}$$

where E_{ii} (i = 1, 2) is the static elastic stiffness, E_{ii}^{adj} is the adjusted elastic stiffness considering strain-rate effect, $\dot{\varepsilon}_{ii}$ is the strain-rate, C_E and P_E are the Cowper-Symonds factors for elastic stiffness, $\varepsilon_{ii}^{\max}$ is the strain at peak stress, $\varepsilon_{ii}^{\max(adj)}$ is the adjusted strain at peak stress, $\dot{\varepsilon}_{ii}^{\max}$ is the maximum strain rate experienced by the element in each respective direction, and C_ε and P_ε are the Cowper-Symonds factors for the strain at peak stress.

Picture frame test has been conducted to determine the shear behavior of Kevlar 49 fabric [6]. In the experiment study, the fabric was sheared at quasi-static loading rate without any pretension and it has very low shear resistance. But in real ballistic scenario, the fabric under impact will experience large tension force during shear deformation. The tension force in the fabric will dramatically influence the shear resistance of the fabric by altering the conditions of the yarn interaction (crimp, yarn compression, normal force at cross-over points), and hence the friction. Duan et al. [19] investigated the friction effects on the ballistic impact behavior of plain weave fabric and found that friction contributed to delaying fabric failure and increasing impact load which allowed the fabric to absorb more energy. If the shear properties of the fabric obtained by picture frame test were used directly in FE simulation, the fabric behaves like a rubber-like material with very large deformation. As the relation between shear properties and tension in fabric is not clear, the shear properties used in the FE simulation was adjusted until the deformation of the fabric in simulation was similar to that of the experiment, and then was optimized to obtain the smallest error in absorbed energy between the simulations and experiments. The in-plane shear stress increment was computed as follows:

$$\Delta\sigma_{12} = \Delta\gamma_{12}G_{12} \tag{4}$$

2.3 Validation of the Continuum Model

To validate the material model, the interaction between the projectile and the fabric was analyzed using the two different modeling configurations (single and multi-layer models) and two aspects of these interactions were closely examined: (a) the absorbed energy by the fabric after the impact, and (b) the temporal evolution and the spatial distribution of fabric deformation and damage. The loss of projectile kinetic energy (absorbed energy), ΔE_{pk} is computed as the kinetic energy of the projectile before impact minus the kinetic energy of the projectile after impact, as follows:

$$\Delta E_{pk} = E_i - E_r = \frac{1}{2} m \left[v_i^2 - v_r^2 \right] \tag{5}$$

where m is the mass of the projectile, v_i is the projectile initial velocity, and v_r is the projectile residual velocity. If presented in percentage, it is given by:

$$\Delta E_{pk}(\%) = (E_i - E_r)/E_i \times 100 = \left(v_i^2 - v_r^2 \right)/v_i^2 \times 100 \tag{6}$$

The percent difference in absorbed energy was computed as:

$$D\ (\%) = \Delta E_{pk}^{\exp}(\%) - \Delta E_{pk}^{sim}(\%) \tag{7}$$

where $\Delta E_{pk}^{\exp}$ is the absorbed energy in experiments, and ΔE_{pk}^{sim} is the absorbed energy in simulation. A positive percent difference corresponds to the FE simulation under-predicting the absorbed energy and a negative percent difference corresponds to the FE simulation over-predicting the absorbed energy.

3. Simulation of Ballistic Impact

3.1 Simulation of Single-Layer Model

Figure 2(a) shows the FE model of the ring and the fabric. The steel ring was modeled with 6.35 mm x 6.35 mm x 25.4 mm hexagonal elements since the ring is not of interest with respect to the FE analysis results. The fabric was modeled with a uniform mesh containing 6.35 mm x 6.35 mm shell elements. One layer of shell elements was used to represent the fabric irrespective of the actual number of fabric layers. The fabric model was meshed using two different parts. The fabric directly in contact with penetrator is given separate part id than rest of the fabric. This type of configuration facilitates tracing of energy balance for this area separately. The shorter, thicker projectile (old) was modeled with 3.81 mm uniform tetrahedral elements for the tip and 5.08 mm x 3.97 mm x 5.14 mm hexahedral elements for the body. The longer, thinner projectile (new) was modeled with 2.54 mm uniform tetrahedral elements for the tip and 3.81 mm x 2.98 mm x 3.80 mm hexahedral elements for the body. Figure 2(b) shows the FE mesh for both projectiles. Both the ring and the projectiles are made of stainless steel, and are modeled as a linear elastic material with Johnson-Cook model to consider the strain rate effect.

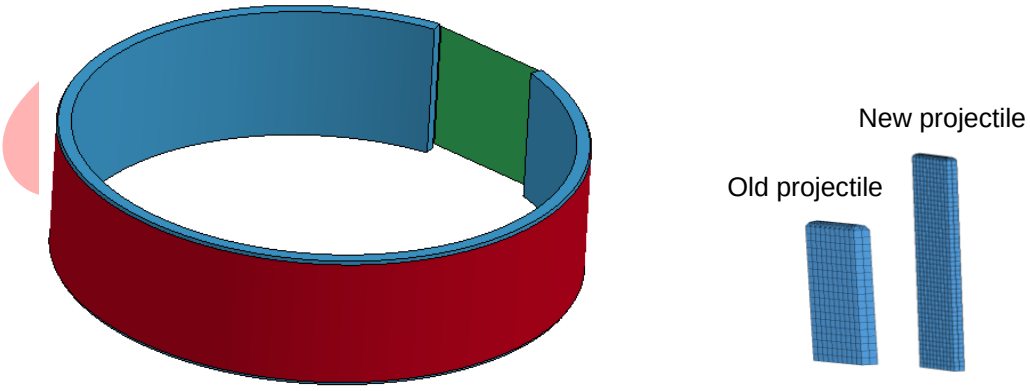

Fig. 2 FE models: (a) ring and single FE layer, (b) projectile FE mesh

Figure 3 shows the comparison of absorbed energy between the experiments and single-layer model simulations. Note that one model predicts the exact absorbed energy in which the projectile was contained by the fabric layers (LG657), three over-predict the absorbed energy with error less than 5%, and eighteen under-predict the absorbed energy with error between 0.4% and 21.1%. When the entire suite of 22 test cases is considered, the FE simulation under-predict the absorbed energy by an average of 5.7% with a standard deviation of 7%. The

model LG656 under-predicts the absorbed energy by the largest amount of 21.1%, followed by LG655 with 19.6% difference. These two are 32-fabric layer test cases with a high projectile velocity relative to the other test cases.
In addition to comparing the absorbed energy, the temporal evolution and the spatial distribution of fabric deformation and damage were also compared between the experiment and the FE simulations. Figure 4 shows the deformations of the experiment and the simulation for LG594. In the test case LG594 the longer and thinner projectile was used. The fabric broke at the impact location and the projectile was bent due to the resistance of the fabric. Overall the simulation captures the general deformed shape and damage of the fabric quite well.

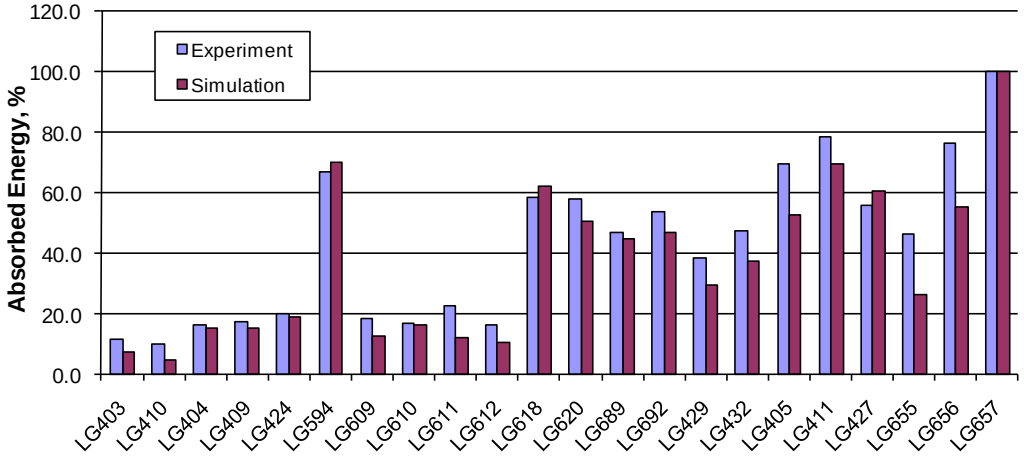

Fig. 3 Comparison of absorbed energy between experiments and single-layer model simulations

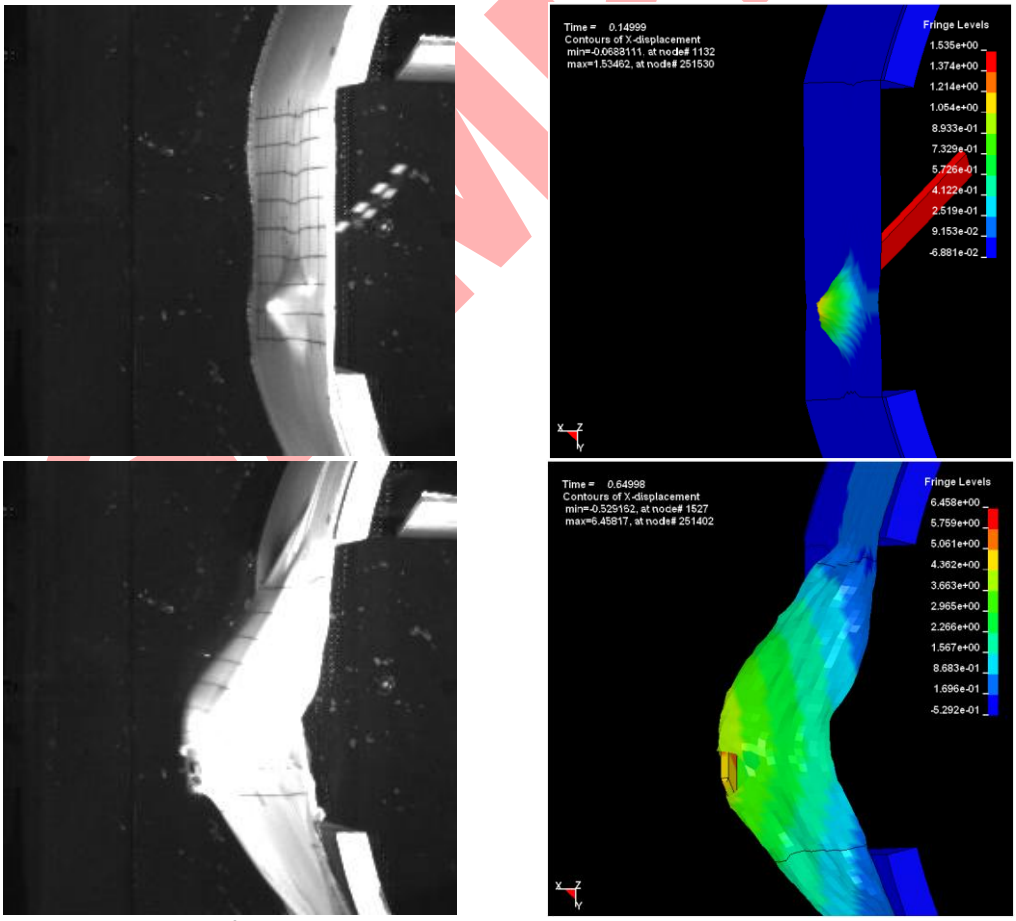

Fig. 4 Deformation comparison between experiment and simulation for LG594

3.2 Simulation of Multi-Layer Model

In the multi-layer model, shell elements were used to represent the fabric and solid elements were used to represent the steel ring and steel projectiles. The fabric was modeled with a uniform mesh containing 6.35 mm x 6.35 mm shell elements. One layer of shell elements was used to represent the four fabric layers. Thus for an test case with 8 fabric layer, there will be two FE layers with shell element thickness of one fabric layer multiplied by 4, or 0.28 mm x 4 = 1.12 mm. With this methodology, the friction between the fabric layers can also be considered. In the model the center of the shell elements was placed at a distance of one half the thicknesses of shell element away from the ring and one shell element away from adjacent shell layer to facilitating contact between them at the start of the analysis. The steel ring and projectiles were modeled in the same way as in the single-layer model. All the simulations of the multi-layer model were run using the same material properties as the single layer model. Figure 5 shows the FE model of the ring and the fabric for a 16 fabric-layer (4 FE-layer) model.

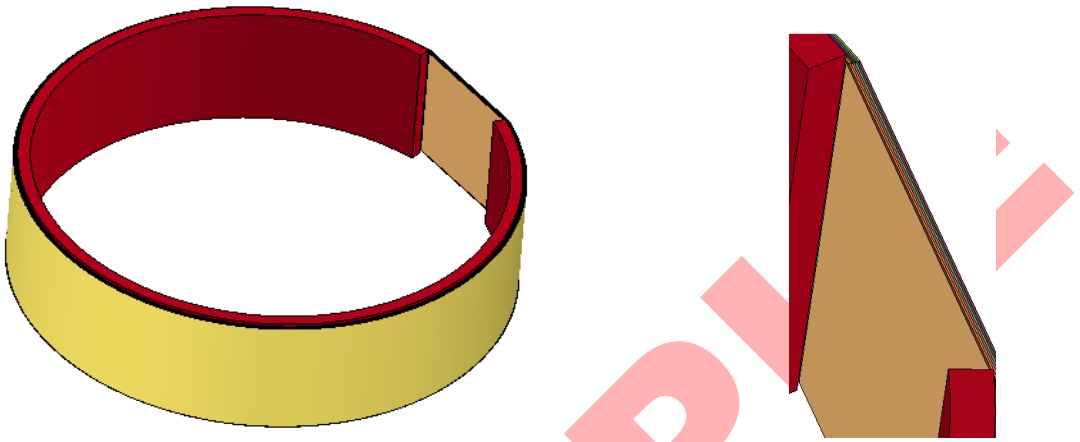

(a) (b)

Fig. 5 Multi-layer FE model of the ring and the fabric: (a) overall view, (b) close-up view of the fabric

Figure 6 shows the comparison of absorbed energy between the experiments and multi-layer model simulations. The test cases LG403, LG410, and LG618 are excluded in the analysis because LG403 and LG410 only have four layers of fabric (one FE-layer) and in LG618 the projectile hits the fabrics in plat, causing significant bending of the projectile during impact. Note that one simulation predicts the exact absorbed energy in which the projectile was contained by the fabric layers (case LG657), and eighteen simulations under-predict the absorbed energy with error between 1.9% and 37%. When the 19 test cases are considered, the FE simulation under-predicts the absorbed energy by an average of 14.5% with a standard deviation of 11.2%. Similar to the single layer model, the temporal evolution and the spatial distribution of fabric deformation and damage were also compared between the experiment and the multi-layer FE simulation. Figure 7 shows the deformations of the experiment and the simulation for test case LG656. The projectile penetrates the fabric layers and the simulated deformation of the fabrics follows the similar pattern to the experiment.

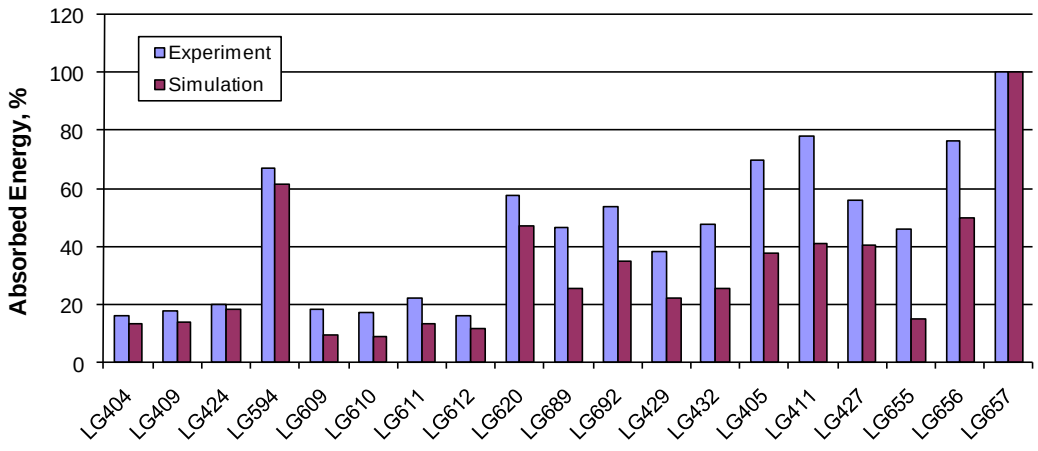

Fig. 6 Comparison of absorbed energy between experiments and multi-layer model simulations

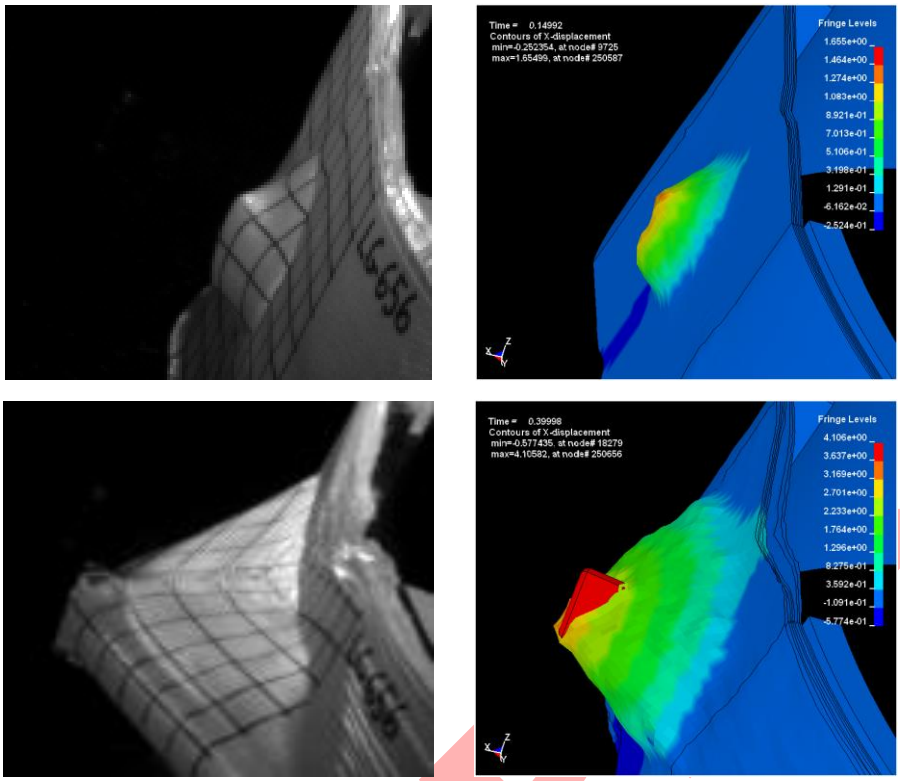

Experiment Simulation

Fig. 7 Deformation comparison between experiment and simulation for LG656

3.3 Comparison of Single-Layer and Multi-Layer Models

The comparison between the LS-DYNA simulations using single-layer and multi-layer models and the experiments is listed in Table 1. The single-layer model under-predicts 18 out of the 22 models and the percent different in the absorbed energy increases with increasing number of fabric layers (increasing thickness of FE layer). The multi-layer model under-predicts 18 out of the 19 models, and the percent different in the absorbed energy also increases with increasing number of fabric layers, as shown in Figure 8. The possible reason is that the outer layers of FE model break prematurely, resulting in relative less resistance again the projectile when comparing with the models with less FE layers. The single-layer model performs better than the multi-layer model as the single-layer model predicts the ballistic tests with less error and standard deviation in terms of the percent difference in absorbed energy. On the average, both of the models under-predict the absorbed energy and are conservative.

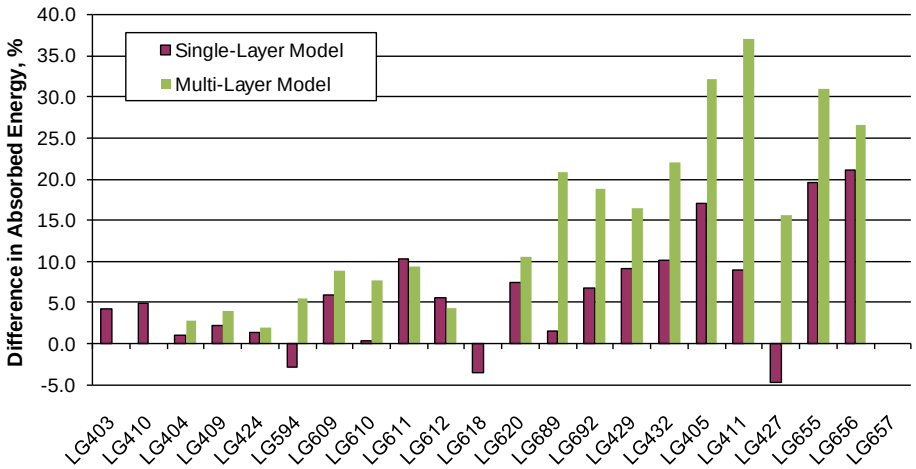

Fig. 8 Comparison of the percent difference in absorbed energy between the single-layer and multi-layer models

Table 1 Comparison between experiments and FE simulations for single-layer (SL) and multi-layer (ML) models

Model	$\Delta E_{pk}^{\exp}$ (%)	ΔE_{pk}^{sim} (%) (SL)	D (%)	ΔE_{pk}^{sim} (%) (ML)	D (%)
LG403	11.3	7.1	4.2	-	-
LG410	9.8	4.9	4.9	-	-
LG404	16.1	15.1	1.0	13.3	2.8
LG409	17.6	15.3	2.3	13.7	3.9
LG424	20.1	18.8	1.3	18.2	1.9
LG594	67.0	69.9	-2.9	61.5	5.5
LG609	18.4	12.5	5.9	9.6	8.8
LG610	16.9	16.5	0.4	9.2	7.7
LG611	22.4	12.1	10.2	13.1	9.3
LG612	16.1	10.6	5.5	11.8	4.3
LG618	58.4	61.9	-3.5	-	-
LG620	57.8	50.3	7.5	47.2	10.6
LG689	46.6	45.0	1.6	25.7	20.9
LG692	53.7	46.8	6.8	34.9	18.8
LG429	38.4	29.3	9.1	22	16.4
LG432	47.4	37.3	10.1	25.4	22
LG405	69.6	52.6	17.1	37.5	32.1
LG411	78.2	69.3	8.9	41.2	37
LG427	56.0	60.7	-4.7	40.5	15.6
LG655	46.1	26.5	19.6	15.1	31
LG656	76.5	55.4	21.1	49.8	26.6
LG657	100.0	100.0	0.0	100	0
Average			5.7		14.5
Minimum			-4.7		0.0
Maximum			21.1		37.0
Std. Dev.			7.0		11.3

3.4 Sensitivity Analysis

A sensitivity analysis of the material model was performed to determine the multi-layer model's sensitivity to the failure strain of the fabric and the friction coefficients of fabric-to-fabric and ring/projectile-to-fabric. The failure strain of the fabric used in the material model was 0.35 for the shell elements. Simulations of all the test cases were run using alternative values of 0.40 and 0.5. Figure 9(a) shows the comparison of the difference in absorbed energy when the different failure strain values are used. Note that there is no difference for all the case when the values of 0.40 and 0.50 are used for the failure strain of elements, and very small difference for the majority of the cases when 0.35 is used. Four difference cases have been carried out to study the effect of friction coefficients of the steel ring/projectile to fabric, and the fabric to fabric, as listed in Table 2. The difference in the absorbed energy varies when different coefficients of friction are used in the simulation, as shown in Figure 9(b). Note that the case LG656 is most sensitive to the friction coefficient compared with other cases, followed by LG427 and LG594.

Table 2 Case study of the effect of friction coefficients

	case 1	case 2	case 3	case 4
fabric-to-fabric	0.2	0.3	0.3	0.4
ring/projectile-to-fabric	0.1	0.1	0.2	0.2

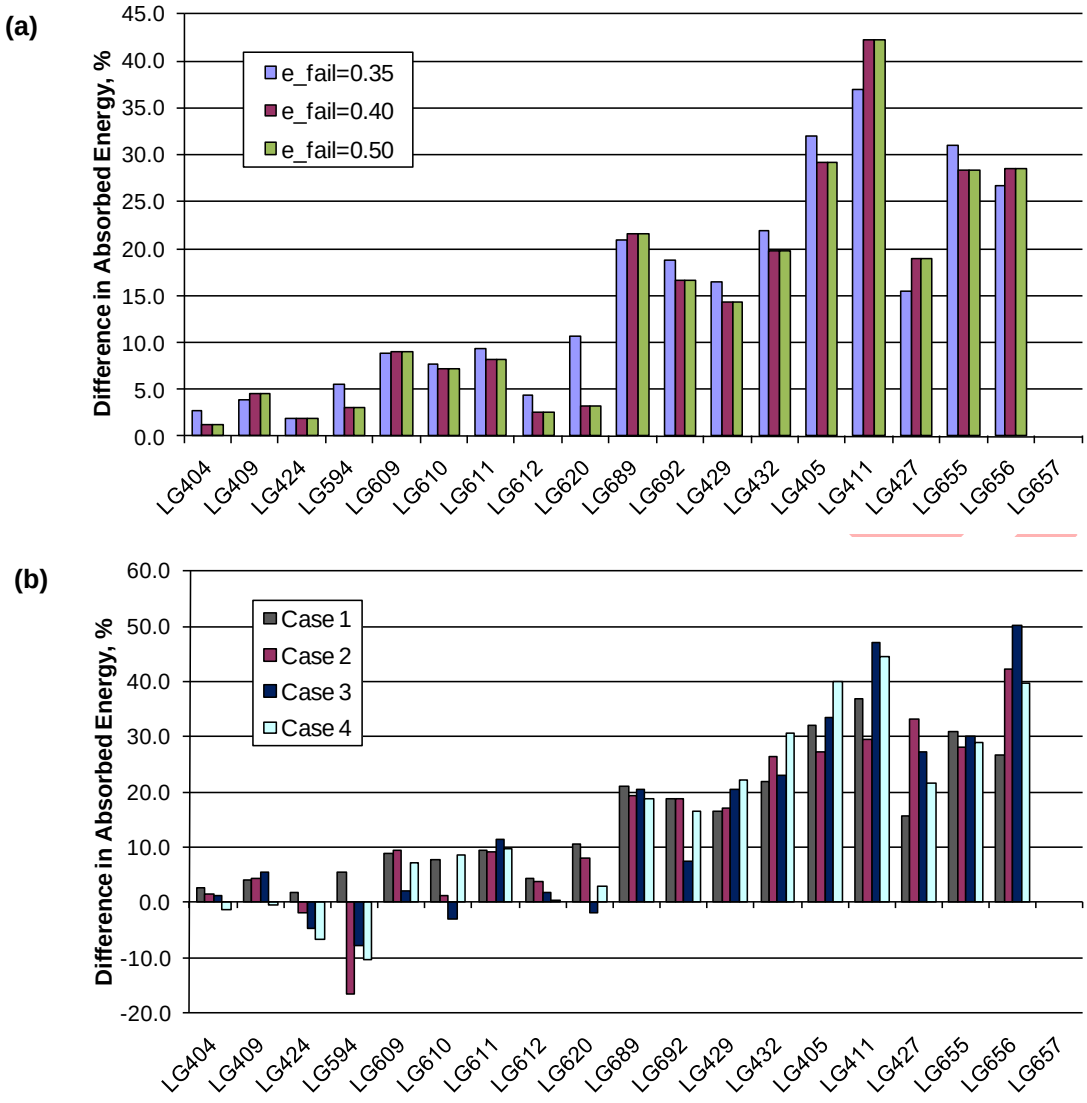

Fig. 9 Comparison of the difference in absorbed energy with different (a) failure strains and (b) coefficients of friction

4. Conclusions

The continuum model developed in previous research has been improved by modifying the stress-strain constitutive behavior and the shear properties. The material model was validated by comparing the FE simulation with the NASA ballistic test results. Both single and multi-layer models were generated in the modeling configuration. The single layer model is computationally efficient and predicts the ballistic tests with less error than the multi-layer model, while the latter is able to consider the friction between fabric layers. The models are validated by comparing the residual velocity of the projectile and the absorbed energy by the fabric after the impact, and the temporal evolution and the spatial distribution of fabric deformation and damage. The sensitivity analysis shows that the material model is more sensitive to the coefficients of friction than to the failure strain within the investigated range.

Acknowledgements

The authors wish to thank William Emmerling, Donald Altobelli and Chip Queitzsch of the Federal Aviation Administration's Aircraft Catastrophic Failure Prevention Research Program for their support and guidance. Funding for this effort was provided by the FAA.

Reference

[1] Grujicic M, Bell WC, Arakere G, He T and Cheeseman BA. A meso-scale unit-cell based material model for the single-ply flexible-fabric armor. Materials and Design, 30, 3690-3704, 2009.

[2] Stahleker Z, Sankaran S, Mobasher B, Rajan SD and Pereira JM. Development of reliable modeling methodologies for engine fan blade-out containment analysis, Part II: finite element analysis. Int J Impact Eng, 36(3), 447-459, 2009.

[3] Bansal S, Mobasher B, Rajan SD and Vintilescu I. Development of fabric constitutive behavior for use in modeling engine fan blade-out events. ASCE Journal of Aerospace Engineering, 22(3), 249-259, 2009.

[4] Sharda J, Deenadayalu C, Mobasher B and Rajan SD. Modeling of multi-layer composite fabrics for gas turbine engine containment systems. ASCE Journal of Aerospace Engineering, 19(1), 38-45, 2006.

[5] Naik D, Sankaran S, Mobasher B, Rajan SD and Pereira JM. Development of reliable modeling methodologies for engine fan blade-out containment analysis. Part I: experimental studies. Int J Impact Eng., 36(1), 1-11, 2009.

[6] Zhu D, Mobasher B, Rajan SD. Characterization of Mechanical Behavior of Kevlar 49 Fabrics. Society for Experimental Mechanics - Annual Conference & Exposition on Experimental and Applied Mechanics, Uncasville, CT, June 13-15, 2011.

[7] Amaniampong G and Burgoyne, CJ. Statistical variability in the strength and failure strain of aramid and polyester yarns. Journal of Material Science, 29, 5141-5152, 1994.

[8] Zhu D, Mobasher B and Rajan SD. Experimental study of dynamic behavior of Kevlar 49 single yarn. Society for Experimental Mechanics - Annual Conference & Exposition on Experimental and Applied Mechanics, v3, p. 542-547, 2010.

[9] Zhu D, Mobasher B, and Rajan SD. Dynamic tensile testing of Kevlar 49 fabrics. ASCE Journal of Materials in Civil Engineering, 2010, in press, http://dx.doi.org/10.1061/(ASCE)MT.1943-5533.0000156.

[10] Zhu D, Mobasher B and Rajan SD. High Strain Rate Testing of Kevlar 49 Fabric. Society for Experimental Mechanics - 11th International Congress and Exhibition on Experimental and Applied Mechanics, v1, p.34-35, 2008.

[11] Zhu D, Mobasher B and Rajan SD. Image Analysis of Kevlar 49 Fabric at High Strain Rate. Society for Experimental Mechanics - 11th International Congress and Exhibition on Experimental and Applied Mechanics, v2, p.986-991, 2008.

[12] Zhu D, Rajan SD, Mobasher B, Peled A and Mignolet M. Modal analysis of a servo-hydraulic high speed testing machine and its application to dynamic tensile testing at an intermediate strain rate. Experimental Mechanics, 2010, in press, http://dx.doi.org/10.1007/s11340-010-9443-2.

[13] Zhu D, Mobasher B and Rajan SD. Characterization of dynamic tensile testing using aluminum alloy 6061-T6 at intermediate strain rates. ASCE Journal of Engineering Mechanics 2010 (accepted).

[14] Zhu D, Peled A and Mobasher B. Dynamic tensile testing of fabric-cement composites. Construction and Building Materials, 25(1), 385-395, 2011.

[15] Zhu D, Mobasher B, Silva FA and Peled A. High Speed Tensile Behavior of Fabric-Cement Composites. International Conference on Material Science and 64th RILEM Annual Week, Proceedings pro075: Material Science - 2nd ICTRC - Textile Reinforced Concrete - theme 1, p. 205-213, 2010.

[16] Silva FA, Zhu D, Mobasher B, Soranakom C and Toledo Filho RD. High speed tensile behavior of sisal fiber cement composites. Materials Science and Engineering: A, 527(3), 544-552, 2009.

[17] Silva FA, Butler M, Mechtcherine V, Zhu D and Mobasher B. Strain rate effect on the tensile behaviour of textile-reinforced concrete under static and dynamic loading. Materials Science and Engineering: A, 528(3), 1727-1734, 2011.

[18] Mechtcherine V, Silva FA, Butler M, Zhu D, Mobasher B, Gao S and Mäder E. Behaviour of strain-hardening cement-based composites under high strain rates. Journal of Advanced Concrete Technology, 9(1), 51-62, 2011.

[19] Duan Y, Keefe M, Bogetti TA and Cheeseman BA. Modeling friction effects on the ballistic impact behavior of a single-ply high-strength fabric. Int J Impact Eng., 31, 996-1012, 2005.